



## Dual-cocatalysts decorated rimous CdS spheres advancing highly-efficient visible-light photocatalytic hydrogen production

Ren-Bin Wei<sup>a</sup>, Zan-Ling Huang<sup>a</sup>, Guang-Hui Gu<sup>a</sup>, Zhu Wang<sup>a,\*</sup>, Lixi Zeng<sup>b</sup>, Yibo Chen<sup>a</sup>, Zhao-Qing Liu<sup>a,\*</sup>

<sup>a</sup> School of Chemistry and Chemical Engineering/ Guangzhou Key Laboratory for Environmentally Functional Materials and Technology/Key Laboratory for Water Quality and Conservation of the Pearl River Delta, Ministry of Education, Guangzhou University, Guangzhou, 510006, PR China

<sup>b</sup> Guangdong Key Laboratory of Environmental Pollution and Health, School of Environment, Jinan University, Guangzhou, 510632, PR China



### ARTICLE INFO

#### Keywords:

CdS  
Dual-cocatalyst  
Hydrogen production  
Photocatalysis

### ABSTRACT

The design and synthesis of robust and efficient photocatalysts for water splitting to generate hydrogen is deemed to be a promising approach for sustainable energy sources. In this work, noble-metal-free nanosstructured ternary NiS/CdS/CdS (NCCS) photocatalysts were elaborately designed and successfully synthesized for high-efficient hydrogen evolution. Taking the advantages of strong absorption and electron buffer property of carbon dots (CDs), as well as merits of internal p-n junction formed between NiS and CdS, the as-prepared NCCS composite shows prominent promotion of hydrogen evolution in comparison with single CdS photocatalyst and binary hybrids (NiS/CdS and CDs/CdS). Remarkably, the optimal ternary hybrid achieves a hydrogen production rate as high as 1444.5  $\mu\text{mol h}^{-1} \text{g}^{-1}$  under visible light irradiation ( $\lambda > 420 \text{ nm}$ ), up to 5.38 times over bare CdS spheres. This work paves a new pathway for the rational design of efficient hybrid photocatalysts toward solar energy conversion to chemical fuels.

### 1. Introduction

To cope with the ever-increasing depletion of fossil fuels and correlative deterioration of environmental conditions, intense research has been devoted to expose green and renewable energy sources [1]. The production of hydrogen over semiconductor-based photocatalytic technology is widely regarded as a prospective pathway for converting solar energy to chemical fuels [2,3]. Based on the mechanism of photocatalytic hydrogen evolution, an ideal photocatalyst should satisfy the following criteria [4–6]: (1) a narrow band gap with high light absorption efficiency, (2) a more negative conduction band edge than standard H<sub>2</sub> reduction potential (H<sup>+</sup>/H<sub>2</sub>O, −0.41 V vs. NHE at pH = 7), (3) effective separation and migration of photo-induced charge carriers and sufficient active reaction sites, and (4) robust activity and stability during long-term hydrogen production. However, up to now, no one single photocatalyst could match well with all the desirability for effective solar water splitting. Therefore, many efforts have been committed to design and prepare semiconductor based hybrid photocatalysts to realize high-efficiency hydrogen generation. Among variety of metal semiconductors, cadmium sulfide (CdS) is a promising candidate with the merits of ideal band gap (2.4 eV) for light harvesting and suitable conduction band edge for H<sub>2</sub> generation [7].

However, due to the serious charge carrier recombination and obstinate photocorrosion, the photocatalytic activity of pristine CdS is still unsatisfactory and needed to be improved urgently [8,9]. In this regard, many strategies including coupling with other semiconductors, loading cocatalyst, and controllable regulating the morphology and structure have been applied to improve the photocatalytic efficiency of CdS catalyst [10–14]. In particular, appropriate cocatalyst modification on CdS material has been proven to be an effective method to greatly improve the photocatalytic activity because the photoinduced charge carriers could be effectively transferred and extracted, thus significantly alleviating unfavorable charge recombination and achieving high charge separation efficiency [15,16].

Recently, carbon dots (CDs) have emerged as a new category of carbon material, which not only show broad absorption spectrum (UV to NIR region) to be potential photosensitizers, but also can act as electron reservoir and donor to effectively improve the photo-induced charge carriers separation [17–19]. Therefore, CDs can contribute to efficiently enhance electron separation and transfer upon photo-excitation, have been frequently employed for improving photocatalytic H<sub>2</sub> generation [20,21]. Moreover, considering the process of the full photocatalytic reaction, photogenerated holes also play a vital role and should be transferred or consumed efficiently to inhibit electron-hole

\* Corresponding authors.

E-mail addresses: [wangzhu@gzhu.edu.cn](mailto:wangzhu@gzhu.edu.cn) (Z. Wang), [lzqgu@gzhu.edu.cn](mailto:lzqgu@gzhu.edu.cn) (Z.-Q. Liu).

recombination and self-oxidation of the photocatalyst. From this point of view, the decoration of cocatalyst for holes separation is a feasible strategy to further enhance the photocatalytic activity. Accordingly, nickel sulfide (NiS), as a robust compound made of earth-abundant elements, has been regarded as a promising cocatalyst for improving the transfer of photo-induced holes [22,23].

Herein, a novel CdS based ternary NiS/CDs/CdS hybrid photocatalysts were elaborately designed and successfully synthesized by a simple two-step strategy, and exhibited superior photocatalytic H<sub>2</sub> production activity under visible light illumination. By virtue of the notable synergistic effect between CDs and NiS dual-cocatalyst, the optimal ternary NiS/CDs/CdS photocatalyst achieved a remarkable H<sub>2</sub>-production rate of 1444.5 μmol g<sup>-1</sup> h<sup>-1</sup> under visible light (> 420 nm), which is about 5.38 and 3.15 times higher than pure CdS and the CDs/CdS photocatalyst, respectively.

## 2. Experimental section

### 2.1. Synthesis of CdS spheres

CdS spheres were prepared via a simple hydrothermal method [24]. In a typical procedure, 1.6 mmol Cd(Ac)<sub>2</sub>·2H<sub>2</sub>O and 8 mmol thiourea were added and dissolved in 20 mL deionized water. The homogeneous solution was transferred to 25 mL stainless steel Teflon lined autoclave and then heated at 140 °C for 24 h. After that, the obtained product were collected and washed in the room temperature.

### 2.2. Synthesis of CDs (carbon dots)/CdS composites

The carbon dots (CDs) was obtained directly from glucose by a one-step alkali assisted ultrasonic treatment [25]. Generally, 0.05 mol glucose was dissolved in 50 mL deionized water and 50 mL equal concentration NaOH was added. The mixed solution was treated ultrasonically for 3 h and the color change to yellowish-brown. Then, a certain amount of HCl was added into raw solution to adjust pH value to 7. Later, 20 mL above solution mixed with 100 mL ethanol little by little under stirring, followed a suitable amount of MgSO<sub>4</sub> was added, subsequently, stored for 24 h. According to the addition of 1, 2, 4 and 8 mL CDs aqueous solution to 100 mg prepared CdS spheres, the obtained CDs modified CDs/CdS composites noted as XCCS.

### 2.3. Fabrication of NiS/CDs/CdS photocatalysts

The deposited NiS on CDs/CdS composites were obtained through precipitated and hydrothermal method and the fabrication process is proposed in Scheme 1. To investigate the effect of NiS deposition content on the photocatalytic activity, a certain amount of CDs/CdS composites with varying Ni(Ac)<sub>2</sub> dissolved in mixed solution contains 96 mL ethyl alcohol and 4 mL deionized water, and then suitable PVP and ammonium hydroxide added reflux heating 20 h at 80 °C. The above-mentioned product put into 50 mL stainless steel Teflon lined autoclave immediately hydrothermal reaction 1 h at 150 °C. After autoclave cooled to room temperature, filtrated and washed several times

with ethyl alcohol and deionized water. Finally, the resulting precipitate was ultrasonic dispersed in 0.5 mol/L Na<sub>2</sub>S solution hydrothermal treatment 6 h at 140 °C, and then washed and dried. The obtained a series of NiS/CDs/CdS photocatalysts defined Y wt% NiS (vs CDs/CdS or CdS) as YNXCCS and YNCS. Following the same procedure described above, the different ratio of binary NiS/CdS photocatalysts were also obtained.

### 2.4. Physicochemical characterizations

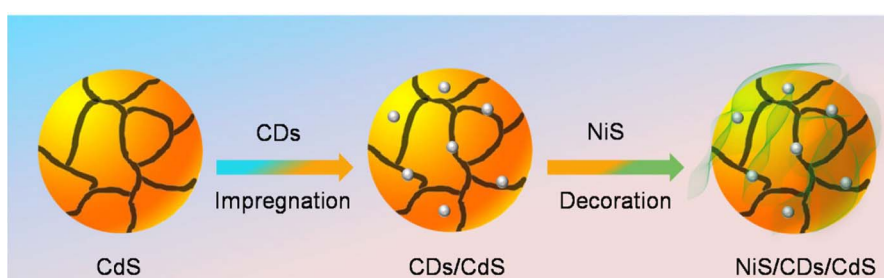
The morphology and structural information of samples were examined by scanning electron microscope (FESEM, JSM-6701F) and transmission electron microscopy equipped with EDS and EDS Mapping (TEM, JEM2010-HR). The phase composition of the samples were detected by Powder X-ray diffraction (XRD, Bruker, D8 ADVANCE) with K<sub>α</sub> irradiation ( $\lambda = 0.15418$  nm). The detailed elemental analysis of the products was investigated with X-ray photoelectron spectroscopy (XPS, Thermo K-Alpha). The UV-vis absorption spectra were carried on Hitachi UV-3010 spectrophotometer using BaSO<sub>4</sub> as a reference. The specific surface area of the materials was calculated by using adsorption data with Brunauer-Emmett-Teller (BET) model. Photoluminescence (PL) spectrum was performed on an F-7000 spectrophotometer.

### 2.5. Photocatalytic hydrogen generation performance

Photocatalytic H<sub>2</sub> evolution experiments of the prepared samples were conducted on a commercial reaction system (LabSolar, Perfect Light Co.). Typically, 100 mg sample was added into a Pyrex reaction cell (250 mL) and dispersed by a constant stirring in 100 mL mixed aqueous solution containing 0.25 M Na<sub>2</sub>S + 0.35 M Na<sub>2</sub>SO<sub>3</sub> as sacrificial agent. A 350 W Xe lamp equipped with a 420 nm cut-off optical filter was used as the light source. Before irradiation, the system was then degassed by using a mechanical pump to ensure a vacuum environment. The solution temperature was controlled at 20 °C by using a water cooling system. The generated H<sub>2</sub> was measured by using an online gas chromatograph (GC7900, Tianmei, Shanghai) equipped with a TCD detector and a molecular sieve 5A column using Ar as the carrier gas.

### 2.6. Electrochemical measurements

The PEC performances were recorded using an electrochemical workstation (CHI 760D, China Chenhua) and an adjustable 350 W Xe lamp with a UV-light cut-off filter ( $\lambda > 420$  nm) as the light source. The as-prepared photocatalysts served as the working electrodes were made by imitating the record (effective area around  $1.5 \times 1.5$  cm<sup>2</sup>) [26], a platinum sheet was used as the counter electrode, and Ag/AgCl electrode (saturated KCl solution) was employed as reference electrode. The 0.25 M Na<sub>2</sub>S + 0.35 M Na<sub>2</sub>SO<sub>3</sub> aqueous solution (pH = 13.56) as the electrolyte. The Mott-Schottky plots of samples measured at a frequency of 1 kHz with an AC imposed bias of 5 mV in the dark. The electrochemical impedance spectra (EIS) were carried out with a sinusoidal perturbation with 10 mV amplitude and frequencies ranging



**Scheme 1.** Schematic illustration for the formation of NiS/CDs/CdS photocatalyst.

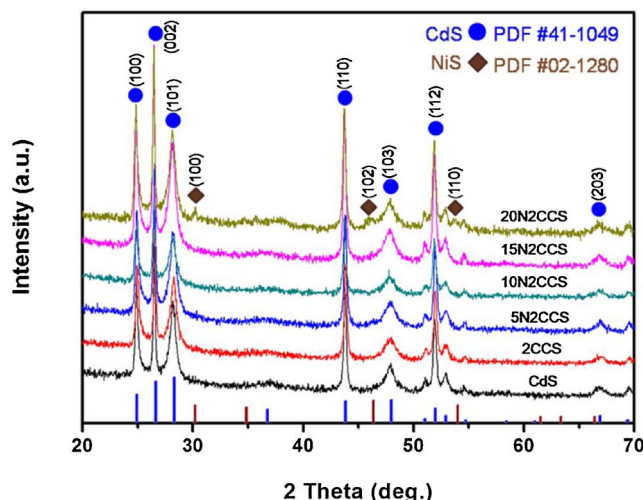


Fig. 1. XRD patterns of the CdS, 2CCS, 5N2CCS, 10N2CCS, 15N2CCS and 20N2CCS.

from 100 kHz to 0.1 Hz at 0.4 V under the illumination.

### 3. Results and discussion

#### 3.1. Phase structure and morphology

X-ray diffraction (XRD) analysis was used to elucidate that the phase structure of CdS-based samples. As presented in Fig. 1, all the samples with several major diffraction peaks centered at 24.8°, 26.5°, 28.2°, 43.7°, 47.8°, 51.8° and 66.8°, which originate from the (100), (002), (101), (110), (103), (112) and (203) planes of the hexagonal CdS phase (JCPDS No. 41-1049), respectively. The absence of characteristic peak for carbons in the XRD spectrum, for the reason that the relative tiny dosage and small size of CDs (seen from Fig. S1). In comparison with pristine CdS and 2CCS, three new diffraction peaks at 30.2°, 46.0° and 53.5° emerged especially in the XRD pattern of 20N2CCS, which can be well-indexed to (100), (102) and (110) facets of NiS (JCPDS No. 02-1280), suggesting the successful loading of NiS in the hybrid photocatalysts [27].

The morphology and internal microstructure of the 10N2CCS ternary hybrid sample were observed by SEM and TEM. As shown in Fig. 2a, the well dispersed CdS spheres have rough surface and an average diameter of about 270 nm. As seen from the high magnification SEM image (Fig. 2b), an ultrathin NiS film deposited on the surface of CdS sphere, which has close contact with CdS. Without obvious morphology difference occur in prepared CdS with different carbon dots amounts (shown in Fig. S2), may be on account of the small size and low content of CDs. Moreover, with the increasing amounts of nickel acetate, the deposited NiS occurred agglomeration and resulting in the vanishing of ultrathin film (Fig. S3). Further careful observation of TEM images (Figs. 2c and 2d) display the successful decoration of NiS and indicate intimate interface conjunction of NiS and CdS. In addition, the interplanar spacing of 0.316 nm corresponds to the (101) planes of CdS, and the compact NiS film with the interplanar spacing of 0.171 nm can be assigned to (110) facet of NiS [28]. The lattice spacing of loading CDs is detected about 0.325 nm, matching (002) plane of graphitic carbon [29]. Elemental mapping patterns (Figs. 2e2h) clearly evidence the presence of C, Ni, Cd and S elements in the sample. These results also reveal that CDs and NiS were successfully deposited on the surface of CdS.

#### 3.2. Surface elemental analysis

XPS was measured to characterize the chemical composition and surface elemental status of the as-prepared ternary NiS/CdS/CdS. In the

Cd 3d XPS spectra as shown in Fig. 3a, the two peaks centered at 405.2 and 412.1 eV are pertained to Cd 3d<sub>5/2</sub> and Cd 3d<sub>3/2</sub>, signifying that the formation of CdS [30]. Meanwhile, the binding energies of S 2p (Fig. 3b) can be detected at about 161.1 eV indexed to sulfide ions in CdS, while peak at 162.2 eV corresponded to the literature for Ni 2p in NiS, further verifying the coexistence of CdS and NiS [31,32]. Fig. 3c displays the high-resolution XPS of C 1s and the typical spectrum could be deconvoluted into three main peaks at around 284.5, 285.8, and 288.4 eV, which are attributed to C–C, C–O and O–C=O bonds, respectively [33]. These three peaks implied the presence of CDs in NiS/CdS/CdS. The observed featured peak of Ni 2p<sub>3/2</sub> located at 858.2 eV in Fig. 3d, which is consistent with the reported values of NiS cocatalyst [34]. Clearly, the EDX spectra (Fig. S4a) and full survey spectra (Fig. S4b) means the NiS/C/CdS sample was successfully synthesized and mainly composed of C, Ni, S and Cd elements.

#### 3.3. Optical properties

To probe the optical properties of all the samples, the UV-vis diffuse reflectance spectroscopy was employed in Fig. 4. The pristine CdS reveals visible light absorption edges at approximately 550 nm, corresponding to a band gap of 2.25 eV. With the introduction of carbon dots, the CDs/CdS exhibits enhanced photo-absorbance intensities in all wavelengths, indicating that carbon dots can serve as a photosensitizer and harvest the light absorption. After coupling with NiS, the markedly increased photoresponse was observed, which can be attribute to intense absorption of NiS under visible light (520–800 nm) [35]. Furthermore, the nearly absorption edge of all samples suggest the loading of co-catalysts NiS and carbon dots can strengthen photoabsorption but not affect the lattice of CdS. In addition, the UV-vis diffuse reflectance spectroscopy of various CDs and NiS loading content were also presented (Fig. S5a and S5b). The similar results demonstrate that CDs and NiS were only deposited on the surface of CdS, but can effectively strengthen visible light absorption to further motivate H<sub>2</sub>-generation activity.

#### 3.4. Photocatalytic hydrogen production and stability tests

The photocatalytic hydrogen production performances of pristine CdS, CDs/CdS, NiS/CdS and NiS/CdS/CdS nanocomposites were assessed in 0.25 M Na<sub>2</sub>S and 0.35 M Na<sub>2</sub>SO<sub>3</sub> aqueous solution as holes sacrificial reagent under simulated visible light irradiation (> 420 nm). Fig. 5a reveals comparable photocatalytic hydrogen production activities of all the samples. As expected, the pristine CdS shows poor H<sub>2</sub> evolution rate of 268.4 μmol g<sup>-1</sup> h<sup>-1</sup> due to the inherent rapid recombination of electron-hole pairs. With the loading of cocatalyst CDs or NiS, the optimal CDs/CdS and NiS/CdS hybrids display the enhanced H<sub>2</sub> evolution rate of 457.9 μmol g<sup>-1</sup> h<sup>-1</sup> and 863.9 μmol g<sup>-1</sup> h<sup>-1</sup>, respectively. Of particular note, the ternary NiS/CdS/CdS catalyst can achieve the maximum hydrogen generation rate of 1444.5 μmol g<sup>-1</sup> h<sup>-1</sup>, which is about 5.38 fold higher than that of pure CdS. Compared to the photocatalytic hydrogen evolution performances of CdS-based ternary composites (Table S1, Supporting information), the as-prepared ternary NiS/CdS/CdS photocatalyst in this work shows superior photocatalytic activity. The strikingly boosted photocatalytic performance demonstrates that both CDs and NiS can weaken the photoinduced charge carrier recombination of the catalyst, and thus, resulting in the remarkable promotion of hydrogen production performance. Moreover, the deposited NiS film and embedded CDs on the CdS sphere surface can simultaneously expand the surface area of hybrids, which may endow composite catalyst with more contact reaction area, hence fulfill preferable photocatalytic performance (Fig. S6, Supporting information). In order to further explore the influence of cocatalyst contents on photocatalytic activity over the CdS composites, binary CDs/CdS and NiS/CdS hybrids with different amounts of CDs and NiS were also synthesized and measured. It is clearly found that the optimal

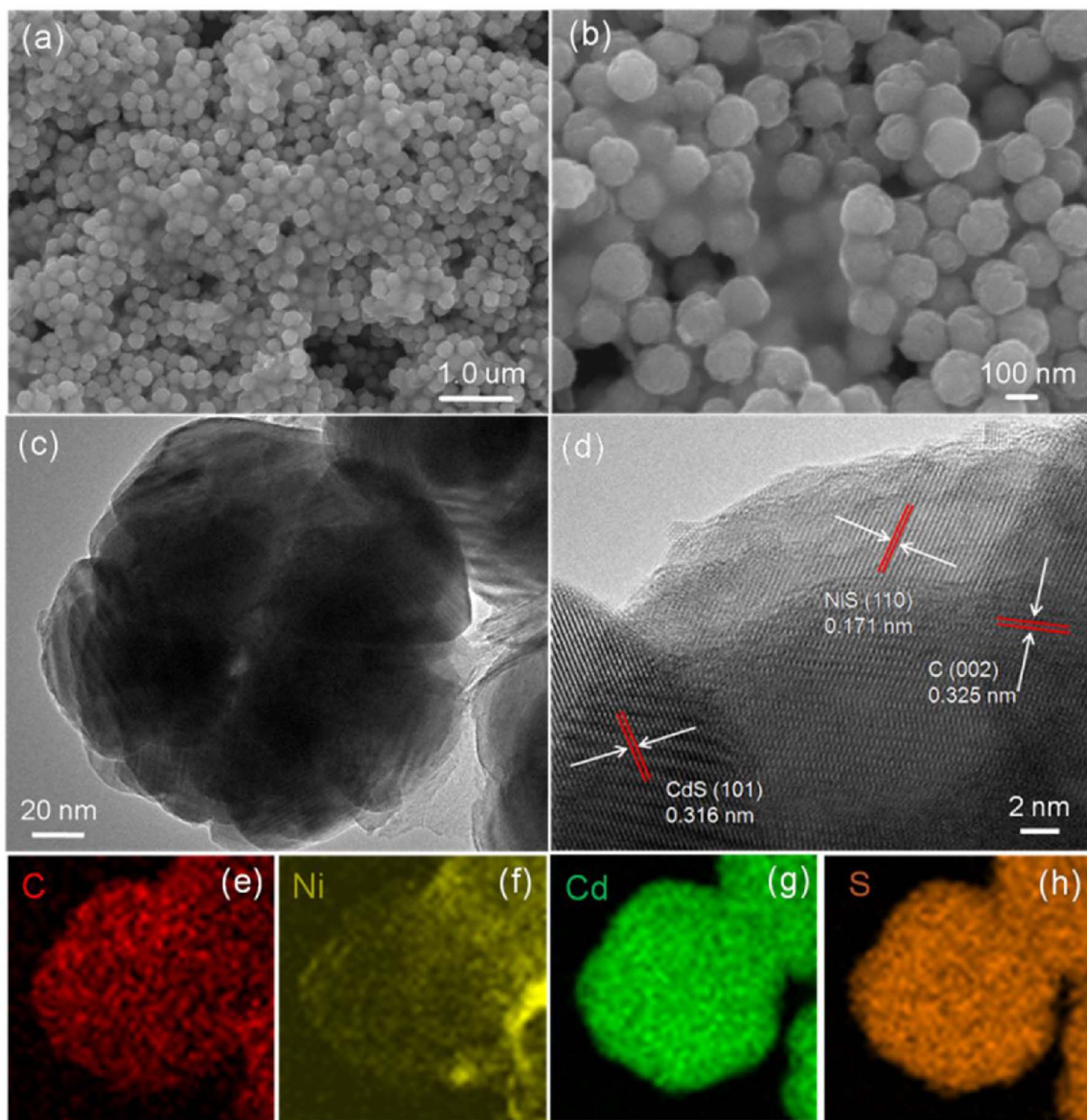


**Fig. 2.** (a, b) SEM, (c) TEM, (d) HRTEM and (e-h) element mapping images of the as-prepared 10N2CCS.

$\text{H}_2$ -production rate of  $457.9 \mu\text{mol g}^{-1} \text{h}^{-1}$  is observed with suitable CDs loading contents of 2 mL (Fig. S7, Supporting information). As we all known, CDs own excellent electron acceptance and donate capability, which can collect and return the photoelectrons of CdS, further prevent the photoelectrons from combining with holes [36,37]. With the increased introduction content of CDs, the obvious decline photocatalytic performances of binary 4CCS and 8CCS were detected. The fact that excess CDs reduce the photocatalytic  $\text{H}_2$ -evolution efficiency gradually can be ascribed to superfluous CDs masked the active reaction sites and block effects [38]. Moreover, the deposition of NiS thin film alone can also promote the rate of hydrogen evolution (Fig. S8, Supporting information). Similarly, the optimum NiS content of binary NiS/CdS hybrids is about 10 Wt% ( $863.9 \mu\text{mol g}^{-1} \text{h}^{-1}$ ) and further increasing the loading of NiS may result in decrease of photocatalytic activity. The probable reason for negative effects of overmuch NiS is that the higher loading amount of NiS clearly agglomerates on the surface of CdS, which could further inhibit the incident light utilization and turn into potential charge recombination centers [39]. Accordingly, the appropriate content of CDs and NiS cocatalyst is influential factor for superior photocatalytic activity in the hybrid photocatalyst system and the synergistic effect of CDs and NiS can efficiently boost the photocatalytic

$\text{H}_2$ -evolution activity. Significantly, the stability and recyclability of photocatalyst is also vital in the practical applications. Fig. 5b shows the photocatalytic cycling test of 10N2CCS under visible light irradiation. After five continuous photocatalytic reaction cycles for 15 h, the ternary 10N2CCS samples maintained stable photocatalytic hydrogen production activity and no distinguishable activity deactivation can be found, further verifying that the ternary 10N2CCS photocatalyst possesses highly photostability and reusability.

### 3.5. Proposed photocatalytic mechanism

In order to deeply understand the improved charge carrier separation and proposed hydrogen production mechanism, Mott-Schottky (M-S) and transient photocurrent responses ( $I-t$ ) measurement were performed. Fig. 6a shows the Mott-Schottky (M-S) plots tested at a frequency of 1 kHz with an AC imposed bias of 5 mV in the dark, the positive slope of CdS and CDs/CdS samples demonstrate that CdS is n-type semiconductor. When CdS combined with NiS, the NiS/CdS and NiS/CDs/CdS composites display an evident p-n junction characteristic in the M-S plot, which a reverse “V-shape” emerged. Hence, it is believed that a certain amount of built-in p-n junctions formed between

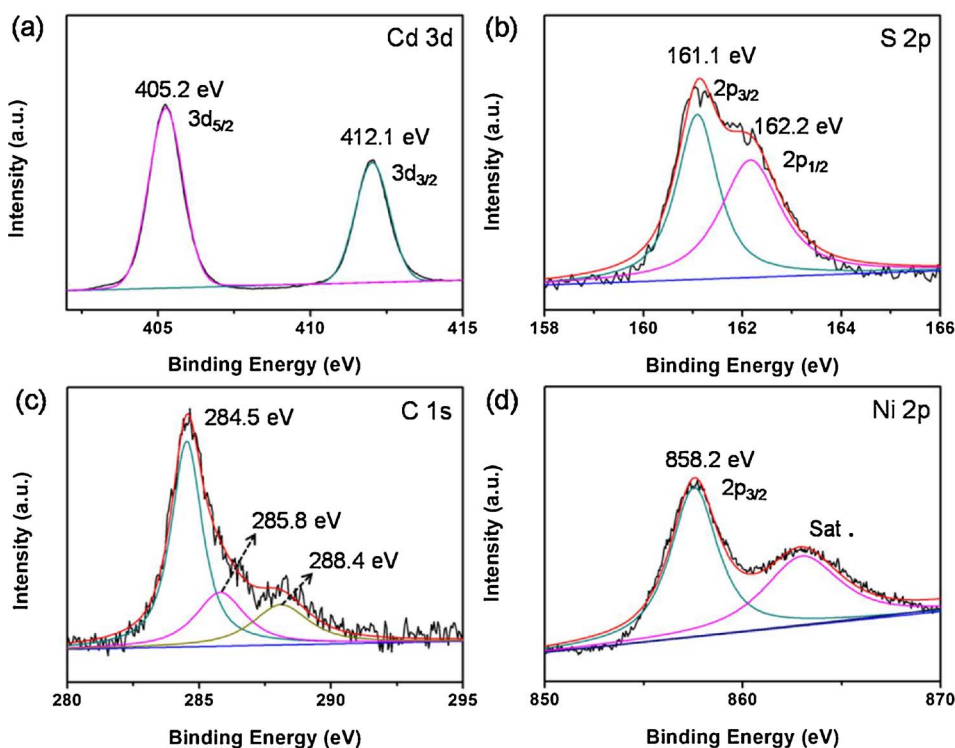


Fig. 3. XPS spectra of the as-prepared 10N2CCS: (a) Cd 3d, (b) S 2p, (c) C 1s, (d) Ni 2p.

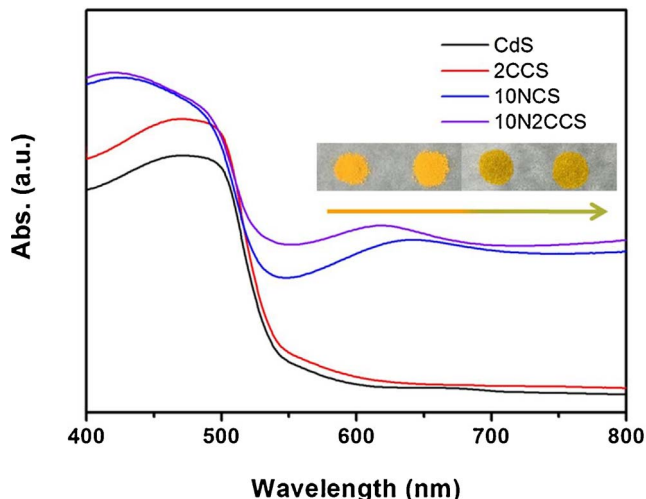


Fig. 4. UV-vis diffuse reflectance spectra of the as-prepared samples.

CdS and adjacent NiS [40]. In addition, the further detailed results also confirm the p-n junction formed between CdS and NiS (Fig. S9). It is well known that a strong internal built-in electrical field can be formed in p-n junction and offer potential driving force to effectively accelerate the separation of photoinduced electron-hole pairs [41–44]. Therefore, the formation of the NiS/CdS p-n heterojunction will greatly restrict the recombination of the photogenerated charge carries in the composite photocatalyst. Then, more available photo-generated electrons and holes could arrive to the photocatalyst surface quickly and participate in reaction, further boost the photocatalytic performance. Moreover, photogenerated charge transfer behavior of all the samples was recorded via (*I-t*) curves (Fig. 6b). The pure CdS shows the lowest photocurrent density owing to the rapid electron-hole recombination, and the enhanced photocurrent value for CDs/CdS suggest that deposition of CDs is in favour of light absorption and electrons extraction. Notably, the ternary NiS/CDs/CdS sample possesses much higher photocurrent response than that of CDs/CdS and NiS/CdS, indicating that the synergistic effects of metal-free CDs and thin NiS as cocatalysts could maximum decrease recombination probability of charge carriers, which in turn support the highest photocatalytic H<sub>2</sub>-production rate of ternary NiS/CDs/CdS photocatalyst. Accordingly, the photocurrent response

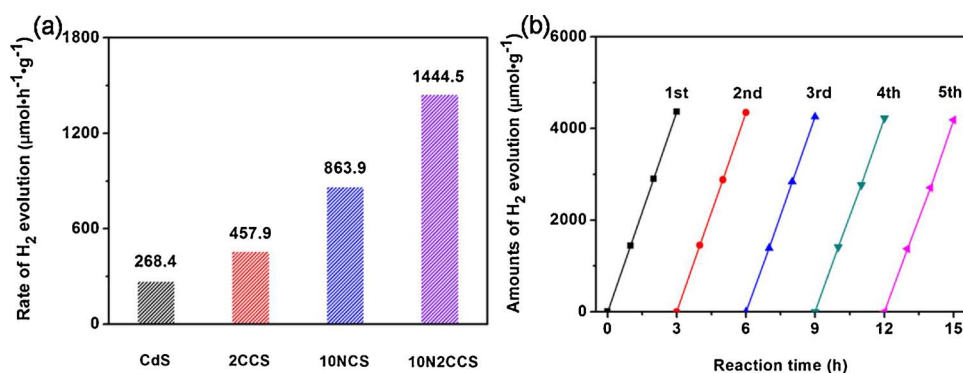


Fig. 5. (a) Hydrogen evolution rates of the as-prepared samples. (b) Recycling test for the hydrogen evolution performance of 10N2CCS.

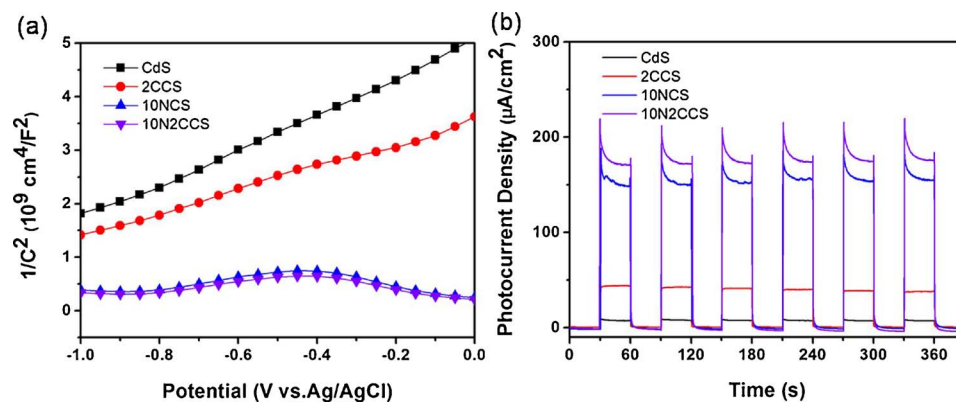


Fig. 6. Mott-Schottky plots (a) at a frequency of 1 kHz with an AC imposed bias of 5 mV and (b) Photocurrent response under visible light illumination ( $> 420 \text{ nm}$ ) of the as-prepared samples.

curves of series of binary NiS/CdS and CDs/CdS hybrids have been also displayed (Fig. S10). The corresponding photocurrent density tendency is match well with the results of measured photocatalytic activity and can prove that the CDs and NiS play positive role in suppressing the recombination of photoinduced electrons and holes.

Furthermore, the photoluminescence (PL) spectra were performed to further understand the separation efficiency and migration behavior of photogenerated electrons and holes. PL spectra of all the samples with excitation wavelength of 480 nm are also presented (Fig. S11). Clearly, the similar emission peaks of different samples at around 725 nm were observed. Furthermore, with the modification of CDs or NiS, the emission intensity of composite samples decreased and NiS/CDs/CdS displayed the lowest emission intensity among all samples. This occurrence can be attributed to the efficient transport of photoexcited charge carrier from CdS to NiS and CDs.

The Electrochemical impedance spectroscopy (EIS) is also a powerful approach to investigate the interfacial charge transfer rate and the smaller arc radiiuses on the EIS Nyquist plots represents the more efficient charge separation [45–47]. The EIS Nyquist plots of different samples were clearly displayed (Fig. 7 and Fig. S12), and the arc radius of NiS/CDs/CdS in the Nyquist plots is smaller than other samples, indicating the lower charge transfer resistance and faster interfacial charge separation. The similar EIS result of samples are in well agreement with the PL, and transient photocurrent measurements strongly reveal that the fastest charge transfer behavior in NiS/CDs/CdS and positive roles of loaded NiS or CDs as effective H<sub>2</sub>-evolution co-catalysts.

Based on the above discussion and analysis, the tentative

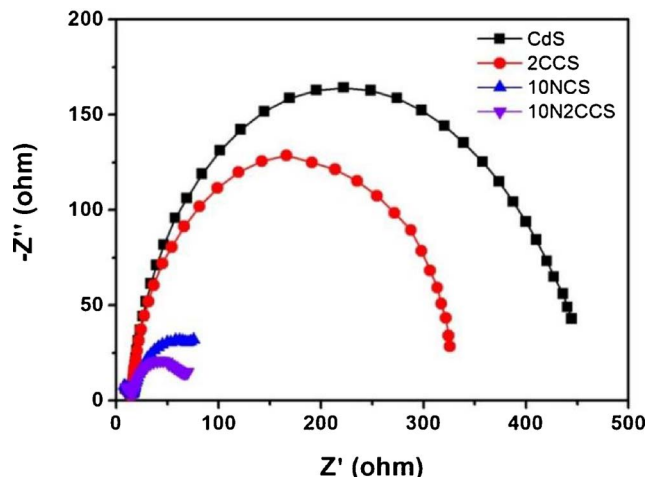


Fig. 7. EIS spectra of different photocatalysts recorded at 0.4 V under visible light illumination.

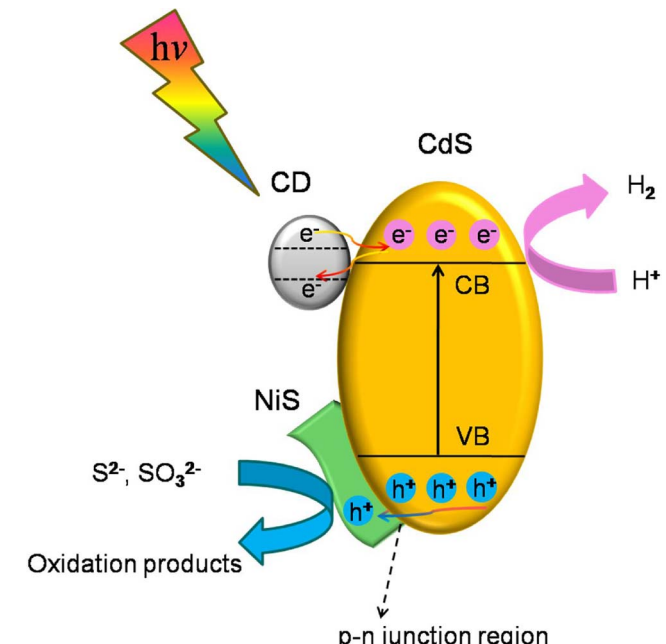


Fig. 8. Schematic diagram of the proposed charge carriers transfer and hydrogen evolution mechanism in 10N2CCS hybrid photocatalysts.

mechanism for enhanced hydrogen generation was proposed in Fig. 8. Under visible light irradiation, CdS was excited easily to create electrons and holes, along with prone to recombination rapidly. The introduction of CDs can play dual positive roles in the hydrogen production process. On the one hand, the CDs could act as electron reservoirs with function of trapping and gathering electron from CB of CdS, which contribute to effective electrons extraction and further suppress the electron-hole pairs recombination. On the other hand, the CDs also serve as photosensitizer and benign electron donator, therein the CDs can increase visible light capture capability and donate the redundant electron return to CdS, facilitate more photoinduced electrons utilized, and consequently promote photocatalytic hydrogen generation performance. Meanwhile, the pre-synthesized n-type CdS can serve as support to load p-type NiS, thus generate many p-n junctions in the interface. These p-n junctions could effectively retard the charge recombination and accelerate the migration of photoinduced holes from CdS to NiS through the inner electric field, while drive photoinduced electrons shift to CdS [48]. Additionally, the NiS thin film deposited on CdS enlarged the reaction area and served as oxidation activity site to exhaust the assembled holes. In other words, the energetic holes excited over CdS will accumulate and consume through

NiS in sacrificial agents. Consequently, the favorable synergistic effect of CDs and NiS for electrons extraction and holes consumption insure the efficient charge separation, thereby leading to significantly promoting the photocatalytic H<sub>2</sub>-production activity over NiS/CDs/CdS dual-cocatalyst hybrid photocatalysts.

#### 4. Conclusions

In summary, a novel ternary NiS/CDs/CdS hybrid photocatalysts are rationally designed and successfully synthesized. By elaborately adjusting the loading amount of CDs and NiS, the optimized 10N2CCS composite exhibited the highest hydrogen production rate of 1444.5 μmol g<sup>-1</sup> h<sup>-1</sup>, which is about 5.38 and 3.15 times higher than the pristine CdS and CDs/CdS photocatalyst, respectively. Notably, in the dual cocatalyst system, the CDs could reserve and return the excited photoelectron of CdS, as well as promote broad light absorption. In addition, the close-connected NiS film can work as oxidation active site and further assemble holes from CdS. Benefitted from the positive synergistic effect between CDs and NiS, the utilization of photogenerated electrons extended while the photogenerated holes can be consumed irreversibly and continually, significantly reduced the recombination probability of photogenerated electron-hole pairs, thus insured the remarkable improvement of photocatalytic hydrogen production activity. This work paves a novel strategy to design robust and cost-effective photocatalysts with high-performance and durability for renewable energy sources.

#### Notes

The authors declare no competing financial interest

#### Acknowledgments

This work was financially supported by Natural Science Foundation of China (Grant No. 21576056, 21576057 and 51608134), the Natural Science Foundations of Guangdong Province (Grant No. 2017A030311016), Science and Technology Research Project of Guangdong Province (Grant No. 2016A010103043), Featured Innovation Project of Guangdong University (Grant No. 2016KTSCX107), Science and Technology Research Project of Guangzhou (Grant No. 201607010232 and 201607010198), Guangzhou University's 2017 Training Program for Young Top-Notch Personnel (BJ201704).

#### Appendix A. Supplementary data

Supplementary material related to this article can be found, in the online version, at doi: <https://doi.org/10.1016/j.apcatb.2018.03.014>

#### References

- [1] K. Zhang, L.Y. Wang, J.K. Kim, M. Ma, G. Veerappan, C.L. Lee, K.J. Kong, H.Y. Lee, J.H. Park, Energy Environ. Sci. 9 (2016) 499–503.
- [2] J. Liu, Y. Liu, N.Y. Liu, Y.Z. Han, X. Zhang, H. Huang, Y. Lifshitz, S.T. Lee, J. Zhong, Z.H. Kang, Science 347 (2015) 970–974.
- [3] S.N. Habireutinger, L. Schmidt-Mende, J.K. Stolarczyk, Angew. Chem. Int. Ed. 52 (2013) 7372–7408.
- [4] H. Zhu, N. Song, H. Lv, C.L. Hill, T. Lian, J. Am. Chem. Soc. 134 (2012) 11701–11708.
- [5] J. Huang, K.L. Mulfort, P. Du, L.X. Chen, J. Am. Chem. Soc. 134 (2012) 16472–16475.
- [6] S. Cao, J. Yu, J. Phys. Chem. Lett. 5 (2014) 2101–2107.
- [7] Y.P. Xie, Z.B. Yu, G. Liu, X.L. Ma, H.M. Cheng, Energy Environ. Sci. 7 (2014) 1895–1901.
- [8] Y.Y. Zhong, G. Zhao, F.K. Ma, Y.Z. Wu, X.P. Hao, Appl. Catal. B Environ. 199 (2016) 466–472.
- [9] X.J. Wang, X.L. Li, C. Liu, F.T. Li, Y.P. Li, J. Zhao, R.H. Liu, G.D. Li, Int. J. Hydrogen Energy 43 (2018) 219–228.
- [10] F. Qiu, Z.J. Han, J.J. Peterson, M.Y. Odoi, K.L. Sowers, T.D. Krauss, Nano Lett. 16 (2016) 5347–5352.
- [11] F.T. Li, S.J. Liu, Y.B. Xue, X.J. Wang, Y.J. Hao, J. Zhao, R.H. Liu, D.S. Zhao, Chem. Eur. J. 21 (2015) 10149–10159.
- [12] R.B. Wei, P.Y. Kuang, H. Cheng, Y.B. Chen, J.Y. Long, M.Y. Zhang, Z.Q. Liu, ACS Sustain. Chem. Eng. 5 (2017) 4249–4257.
- [13] B. Chica, C.H. Wu, Y. Liu, M.W.W. Adams, T.Q. Lian, R.B. Dyer, Energy Environ. Sci. 10 (2017) 2245–2255.
- [14] L. Li, P.C. Wu, X.S. Fang, T.Y. Zhai, L. Dai, M.Y. Liao, Y. Koide, H.Q. Wang, Y. Bando, D. Golberg, Adv. Mater. 22 (2010) 3161–3165.
- [15] H.G. Yu, X. Huang, P. Wang, J.G. Yu, J. Phys. Chem. C 120 (2016) 3722–3730.
- [16] F. Wen, C. Li, Acc. Chem. Res. 46 (2013) 2355–2364.
- [17] Z. Li, L.Y. Zhu, W. Wu, S.F. Wang, L.W. Qiang, Appl. Catal. B Environ. 192 (2016) 277–285.
- [18] H.J. Yu, Y.F. Zhao, C. Zhou, L. Shang, Y. Peng, Y.H. Cao, L.Z. Wu, C.H. Tung, T.R. Zhang, J. Mater. Chem. A 2 (2014) 3344–3351.
- [19] B.M. Martindale, G.M. Hutton, C. Caputo, E. Reisner, J. Am. Chem. Soc. 137 (2015) 6018–6025.
- [20] J.G. Hou, H.J. Cheng, C. Yang, O. Takeda, H.M. Zhu, Nano Energy 18 (2015) 143–153.
- [21] J. Liu, H.C. Zhang, D. Tang, X. Zhang, L.K. Yan, Y.Z. Han, H. Huang, Y. Liu, Z.H. Kang, ChemCatChem 6 (2014) 2634–2641.
- [22] J. Zhang, L.F. Qi, J.R. Ran, J.G. Yu, S.Z. Qiao, Adv. Energy Mater. 4 (2014) 1301925–1301931.
- [23] S. Nandy, T. Hisatomi, G.J. Ma, T. Minegishi, M. Katayama, K. Domen, J. Mater. Chem. A 5 (2017) 6106–6112.
- [24] P.Y. Kuang, P.X. Zheng, Z.Q. Liu, J.L. Lei, H. Wu, N. Li, T.Y. Ma, Small 12 (2016) 6735–6744.
- [25] H.T. Li, X.D. He, Y. Liu, H. Huang, S.Y. Lian, S.T. Lee, Z.H. Kang, Carbon 49 (2011) 605–609.
- [26] J.P. Huo, H.P. Zeng, J. Mater. Chem. A 3 (2015) 17201–17208.
- [27] J.L. Yuan, J.Q. Wen, Y.M. Zhong, X. Li, Y.P. Fang, S.S. Zhang, Wei Liu, J. Mater. Chem. A 3 (2015) 18244–18255.
- [28] Y.C. Liu, Z. Kang, H. Sia, P.F. Lia, S.Y. Cao, S. Liu, Y. Li, S.C. Zhang, Z. Zhang, Q.L. Liao, L. Wang, Y. Zhang, Nano Energy 35 (2017) 189–198.
- [29] J.Y. Qin, H.P. Zeng, Appl. Catal. B Environ. 209 (2017) 161–173.
- [30] P.Y. Kuang, Y.Z. Su, K. Xiao, Z.Q. Liu, N. Li, H.J. Wang, J. Zhang, ACS Appl. Mater. Interfaces 7 (2015) 16387–16394.
- [31] Z.H. Chen, P. Sun, B. Fan, Z.G. Zhang, X.M. Fang, J. Phys. Chem. C 118 (2014) 7801–7807.
- [32] J. Yu, Y. Yu, P. Zhou, W. Xiao, B. Cheng, Appl. Catal. B 156–157 (2014) 184–191.
- [33] S.Y. Zhao, C.X. Li, L.P. Wang, N.Y. Liu, S. Qiao, B.B. Liu, H. Huang, Y. Liu, Z.H. Kang, Carbon 99 (2016) 599–606.
- [34] J.D. Hong, Y.S. Wang, Y.B. Wang, W. Zhang, R. Xu, ChemSusChem 6 (2013) 2263–2268.
- [35] Z. Chen, P. Sun, B. Fan, Z. Zhang, X. Fang, J. Phys. Chem. C 118 (2014) 7801–7807.
- [36] P.Y. Zhang, T. Song, T.T. Wang, H.P. Zeng, Appl. Catal. B Environ. 206 (2017) 328–335.
- [37] S.Y. Lim, W. Shen, Z. Gao, Chem. Soc. Rev. 44 (2015) 362–381.
- [38] J.Q. Wen, X. Li, H.Q. Li, S. Ma, K.L. He, Y.H. Xu, Y.P. Fang, W. Liu, Q.Z. Gao, Appl. Surf. Sci. 358 (2015) 204–212.
- [39] J. Zhang, S.Z. Qiao, L.F. Qia, J.G. Yu, Phys. Chem. Chem. Phys. 15 (2013) 12088–12094.
- [40] F.K. Meng, J.T. Li, S.K. Cushing, M.J. Zhi, N.Q. Wu, J. Am. Chem. Soc. 135 (2013) 10286–10289.
- [41] W.Z. Wang, X.W. Huang, S. Wu, Y.X. Zhou, L.J. Wang, H.L. Shi, Y.J. Liang, B. Zou, Appl. Catal. B Environ. 134–135 (2013) 293–301.
- [42] M. Wang, L. Sun, Z. Lin, J. Cai, K. Xie, C. Lin, Energy Environ. Sci. 6 (2013) 1211–1220.
- [43] H. Li, Y. Zhou, W. Tu, J. Ye, Z. Zou, Adv. Funct. Mater. 25 (2015) 998–1013.
- [44] M. Zhong, T. Hisatomi, Y. Kuang, J. Zhao, M. Liu, A. Iwase, Q. Jia, H. Nishiyama, T. Minegishi, M. Nakabayashi, N. Shibata, R. Niishiro, C. Katayama, H. Shibano, M. Katayama, A. Kudo, T. Yamada, K. Domen, J. Am. Chem. Soc. 137 (2015) 5053–5060.
- [45] K.H. Ye, Z.L. Wang, J.W. Gu, S. Xiao, Y.F. Yuan, Y. Zhu, Y.M. Zhang, W.J. Mai, S.H. Yang, Energy Environ. Sci. 10 (2017) 642–649.
- [46] Z.M. Bai, X.Q. Yan, Y. Li, Z. Kang, S.Y. Cao, Y. Zhang, Adv. Energy Mater. 6 (2016) 1501459–1501466.
- [47] D. Chen, K. Wang, W. Hong, R. Zong, W. Yao, Y. Zhu, Appl. Catal. B Environ. 166 (2015) 366–373.
- [48] P.H. Yang, X. Xiao, Y.Z. Li, Y. Ding, P.F. Qiang, X.H. Tan, W.J. Mai, Z.Y. Lin, W.Z. Wu, T.Q. Li, H.Y. Jin, P.Y. Liu, J. Zhou, C.P. Wong, Z.L. Wang, ACS Nano 7 (2013) 2617–2626.